Journal of Nonlinear Optical Physics & Materials
Vol. 35, No. 2 (2026) 2550015 (26 pages)

DOI: 10.1142/S0218863525500158

Beyond the symmetry: Exploring the nonlinear dynamics of 1D and 2D $\mathcal{PT}$-symmetric sinusoidal systems

C. P. Jaseera *,† and K. Aysha Muhsina *,‡

*Department of Physics,
Government Arts and Science College,
Kozhikode 673018, Kerala, India

†Department of Physics,
Government Arts and Science College,
Nadapuram 673506, Kerala, India
‡muhsina.mtl@gmail.com

Received 4 November 2024
Accepted 26 January 2025
Published 14 March 2025

This work investigates the evolution of nonlinear eigenmodes in one-dimensional (1D) and two-dimensional (2D) optical systems with $\mathcal{PT}$-symmetric sinusoidal complex potentials, which supports real eigenvalue spectra up to the symmetry-breaking threshold. Numerical results show that in 1D and 2D systems, when nonlinearity increases, the threshold potential decreases. However, a deeper real potential increases the threshold in 1D, while it destabilizes the 2D optical beam as illustrated in the stability charts. Below this threshold, eigenfunctions exhibit symmetric behavior with smooth phase variations and no abrupt changes in energy flux. In contrast, the broken $\mathcal{PT}$-symmetric phase results in asymmetric eigenfunctions, indicating the instability. Stability analysis using Bogoliubov–de Gennes (BDG) matrix method and the propagation dynamics confirmed that eigenstates remain stable under small perturbations below the threshold but lose stability once the imaginary potential exceeds the threshold. Understanding the behavior of eigenmodes in $\mathcal{PT}$-symmetric potentials enables advanced control over beam profiles, potentially benefiting high-precision sensors, lasers, and optical trapping.

Keywords: 2D nonlinear system; bright soliton; $\mathcal{PT}$-symmetric potential; stability analysis; energy flux.

1. Introduction

The exploration of parity-time ($\mathcal{PT}$) symmetric structures has significantly deepened our understanding of quantum mechanics and revolutionized the field of optics.[1] Since Bender and Boettcher's seminal work,[2,3] it has been established that $\mathcal{PT}$-symmetric Hamiltonians can have real eigenvalue spectra despite being non-Hermitian. The parity operator $\hat{P}$ turns $\hat{p}$ to $-\hat{p}$, $\hat{x}$ to $-\hat{x}$, and the time reversal

‡Corresponding author.

operator $\hat{T}$ shifts $\hat{p}$ to $-\hat{p}$, $\hat{x}$ to $\hat{x}$, and i to $-i$, where $\hat{p}$ and $\hat{x}$ are momentum and position operators. The Hamiltonian of a system is stated as $\hat{H} = \frac{\hat{p}^2}{2m} + V(x)$, in which m is mass and $V(x)$ the complex potential. Let the Hamiltonian be $\mathcal{PT}$-symmetric when $\hat{P}\hat{T}\hat{H} = \hat{H}\hat{P}\hat{T}$ is satisfied, which demands that $V(x) = V^*(-x)$.[4,5] This enchanted phenomenon occurs when the real part of the potential is an even function of the position while the imaginary part, which represents gain and loss, is an odd function.[6–11] The introduction of $\mathcal{PT}-$ symmetry in optics stimulated the development of new optical lattices, lasers, meta-materials and broadened the scope of optical physics and engineering.[12,13]

One of the most significant aspects of the optical $\mathcal{PT}$-symmetric structures is the presence of a phase transition, specifically for periodic $\mathcal{PT}$ potentials.[6] All eigenvalues are real under this threshold. However, as the magnitude of the gain–loss term crosses this limit, complex eigenvalues develop, and the intensity of the light beam varies throughout the propagation.

Incorporating $\mathcal{PT}$-symmetry in soliton systems is a rich and expanding area of research, where solitons are reinforced beams that propagate in conservative nonlinear media by balancing spatial diffraction and self-focusing/defocusing nonlinearity.[14,15] In systems like $\mathcal{PT}$-symmetric systems, which represent a specialized category of dissipative media, the spatially balanced gain and loss are balanced to satisfy the parity-time ($\mathcal{PT}$) symmetry condition. This balance ensures that the system behaves as a boundary between fully conservative systems, where energy is preserved, and generic dissipative systems, where energy is either lost or gained overall. Researchers can create new forms of solitons in nonlinear $\mathcal{PT}$-symmetric system with distinct properties that can be used in optical communications, nonlinear optics, and other fields of physics by leveraging the gain–loss balance in these systems. These structures, which are identified by a precise balance of gain and loss, thus reveal new symmetry aspects that challenge the norms of physics concepts and open new opportunities for developing unique photonic devices with better functionality.

Nonlinear interactions in fibers are usually cubic, although some structures produce both the cubic and quintic (CQ) nonlinearities. This demonstrates that the refractive index of the medium is modified by both cubic (Kerr) and quintic elements of the beam intensity as $n(I) = n_0 + n_2 I + n_4 I^2$, where n_0 is the linear refractive index, n_2 is the coefficient of the cubic nonlinearity, n_4 is the coefficient of the quintic nonlinearity, and I is the intensity of the light. In double-doped optical fibers, where the kind of dopant varies throughout the fiber, the values of the cubic and quintic elements that govern the nonlinearities can be modulated.[16–20]

Solitons are divided into one-dimensional (1D) and two-dimensional (2D) types based on their spatial localization. 1D solitons are stable, localized wave packets in a single spatial dimension, commonly observed in optical fibers where they balance nonlinearity and diffraction. In contrast, 2D solitons, localized in two spatial dimensions, carry complex dynamics and are more challenging to stabilize due to their susceptibility to collapse. These solitons play a crucial role in planar waveguides

and photonic crystals. In recent times, researchers explored optical solitons in $\mathcal{PT}$-symmetric non-conservative systems using coupled Kerr and quintic nonlinearities.[21–23] The system experiences a phase shift that causes $\mathcal{PT}$-symmetry breakdown, above a specific complex potential threshold.[24]

Several significant theoretical studies and experimental investigations have advanced the understanding and application of $\mathcal{PT}$-symmetric systems. Key contributions include the double refraction, and power oscillations in $\mathcal{PT}$-symmetric system.[25] An overview of the theoretical framework and implementation strategies for $\mathcal{PT}$-symmetry in optics[26] along with the exploration of spontaneous $\mathcal{PT}$-symmetry breaking in disordered optical lattices[7] has been discussed. Experimental work has provided insight into $\mathcal{PT}$-symmetry breaking in AlGaAs materials[6] and the propagation of optical beams in iron-doped $LiNbO_3$.[5] Further studies have delved into wave mechanics in $\mathcal{PT}$-symmetric periodic systems[10] such as jamming anomalies during power transfer in $\mathcal{PT}$-symmetric coupled modes with cubic nonlinearity.[27] There are some works which analyzed the stability of cubic eigenmodes within $\mathcal{PT}$-symmetric parabolic potential fields,[28] beam propagation in defocusing nonlinear $\mathcal{PT}$-symmetric Scarff-II potential system,[29,30] stability of dark solitons in $\mathcal{PT}$-symmetric Gaussian and super-Gaussian potential,[31,32] nonlinear eigenmodes in hyperbolic complex potential,[33] stability of nonlinear waves in $\mathcal{PT}$-symmetric quartic harmonic potential,[34] instability of eigenmodes in $\mathcal{PT}$-symmetric Rosen–Morse system and stable beam propagation in modified Rosen–Morse system,[24,35] the input power-dependent switching dynamics in with $\mathcal{PT}$-symmetric Scarf-II barrier potential coupled system,[36] etc. These works have been pivotal in advancing the field of $\mathcal{PT}$-symmetric nonlinear systems.

Following the exploration of 1D solitons, 2D solitons have garnered significant attention due to their dynamics and potential applications in advanced photonic systems. Numerous studies have investigated the formation, stability, and behavior of 2D solitons in various nonlinear $\mathcal{PT}$-symmetric systems which include the stability of 1D and 2D beams in $\mathcal{PT}$-symmetric saturable nonlinear medium supported with Scarff-potential,[37] stability of $(2+1)$-dimensional solitons in spatiotemporal dispersive medium with quadratic–cubic nonlinearity,[38] a novel genre of 1D and 2D nonlinear modes and the study of its bandgap structure present in $\mathcal{PT}$-symmetric wells and lattices,[11] the development and propagation of $(2+1)$D stationary solutions in the $\mathcal{PT}$-symmetric potential,[39] gap solitons supported by 2D $\mathcal{PT}$-symmetric optical lattices with fourth-order diffraction,[40] exploration of self-defocusing beam in $\mathcal{PT}$-symmetric 1D and 2D systems supported by Scarff-II potential,[41] the existence of symmetry breaking of optical solitons in $(1+1)$D $\mathcal{PT}$-symmetric CQNLS system with the fourth-order diffraction,[42] propagation of beam in 2D CQ sytem with annular potential,[43] the propagation dynamics of 2D multi-peak solitons in the optical lattices,[44] numerical simulation of 2D solitons in nonlocal nonlinear $\mathcal{PT}$-symmetric Scarff-II system,[45] stability domains of 2D gap solitons in cubic quintic PT symmetric system with fractional diffraction,[46] localized eigenmodes in 2D $\mathcal{PT}$-symmetric Rosen–Morse system, etc.

This work explores 1D and 2D fundamental and excited (overtone) eigenmodes in a self-focusing CQ nonlinear $\mathcal{PT}$-symmetric sinusoidal potential field. This study investigates how the imaginary field affects $\mathcal{PT}-$ symmetry collapse. Section 2 explains the physical model that represents the system and discusses how the real and imaginary parameters of complex potential and the order of the nonlinear function affect the eigenvalue spectra of 1D and 2D systems. Section 3 analyzes the stability of the beam under perturbation and Sec. 4 goes over the stability of the beam during propagation both in 1D and 2D systems. Section 5 concludes.

2. Mathematical Framework and System Dynamics

The evolution of complex wave functions in nonlinear media is described by the nonlinear Schrodinger equation (NLSE) having the form in 1D CQ system as

$$i\frac{\partial\psi(x,z)}{\partial z}+\zeta\frac{\partial^2\psi(x,z)}{\partial x^2}+\beta|\psi(x,z)|^2\psi(x,z) + \beta_2|\psi(x,z)|^4\psi(x,z)+V(x)\psi(x,z)=0, \tag{1}$$

where β and β_2 are Kerr and quintic nonlinearities, respectively, ζ stands for the coefficient of diffraction, $V(x)$ is the complex $\mathcal{PT}$-symmetric potential field, and $\psi(x,z)$ is the amplitude of the beam which is propagating along z direction and confined along x direction. If the nonlinearity implied by β and β_2 is greater than zero, the medium is self-focusing, whereas β, $\beta_2<0$ suggest a defocusing one. In 2D nonlinear system, NLSE has the following form:

$$i\frac{\partial\psi(x,y,z)}{\partial z}+\zeta\left(\frac{\partial^2\psi(x,y,z)}{\partial x^2}+\frac{\partial^2\psi(x,y,z)}{\partial y^2}\right)+\beta|\psi(x,y,z)|^2\psi(x,y,z) + \beta_2|\psi(x,y,z)|^4\psi(x,y,z)+V(x,y)\psi(x,y,z)=0, \tag{2}$$

where $\psi(x,y,z)$ is the spatial profile of the beam, describing how its amplitude and phase modify along the propagation path(z) and across the transverse plane(x,y). The optical beam is driven by the $\mathcal{PT}$-symmetric potential of the form in 1D system

$$V(x)=V_0\cos^2(x)+iW\sin(x)\cos(x), \tag{3}$$

where V_0 and W are the coefficients of the real and imaginary components of the potential, respectively. In 2D system, it is

$$V(x,y)=V_0[\cos^2(x)+\cos^2(y)]+iW[\sin(x)\cos(x)+\sin(y)\cos(y)]. \tag{4}$$

The real part of the potential stands for the waveguiding and the imaginary part for the gain/loss (in the system) that constitutes the potential. Variation of the potential as a function of spatial coordinate is given in Fig. 1. In this work, we examine how the system parameters affect the stationary solution of the NLSE in 1D and 2D systems by analyzing the eigenvalues and eigenfunctions. For this,

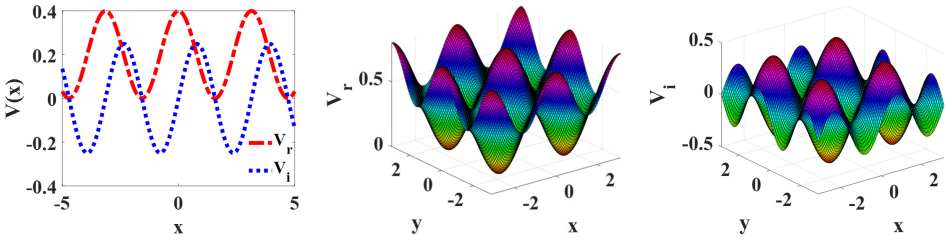

(a) $V_0 = 0.4$, $W = 0.5$ (b) $V_0 = 0.4$, $W = 0.5$ (c) $V_0 = 0.4$, $W = 0.5$

Fig. 1. The evolution of complex $\mathcal{PT}$-symmetric potentials for $V_0 = 0.4$, $W = 0.5$ (a) V_r and V_i of 1D potential (b) V_r of 2D potential (c) V_i of 2D potential.

consider a stationary solution for eigenvalue equations, having the following form:

$$\psi(x, z) = \phi(x)e^{-i\mu z} \tag{5}$$

and

$$\psi(x, y, z) = \phi(x, y)e^{-i\mu z}. \tag{6}$$

$\phi(x)$ is a complex wave field independent of the propagation coordinate z and defined in spatial coordinate x while $\phi(x, y)$ is stationary profile in $x - y$ domain and μ is the constant of propagation with both real and imaginary components.

$$\mu = \mu_r + i\mu_i. \tag{7}$$

The function $\phi(x)$ modifies NLSE to the stationary nonlinear eigenvalue equation which is comprised of one independent variable x as

$$-\zeta\frac{d^2\phi(x)}{dx^2} - \beta|\phi(x)|^2\phi(x) - \beta_2|\phi(x)|^4\phi(x) - V(x)\phi(x) = \mu\phi(x) \tag{8}$$

and

$$\begin{aligned}&-\zeta\nabla^2\phi(x, y) - \beta|\phi(x, y)|^2\phi(x, y)\\ &\quad - \beta_2|\phi(x, y)|^4\phi(x, y) - V(x, y)\phi(x, y) = \mu\phi(x, y)\end{aligned} \tag{9}$$

The trial function taken for $\phi(x)$ and $\phi(x, y)$ is a Gaussian

$$\phi(x) = A\exp\left[\frac{-x^2}{a^2} + \frac{ibx^2}{2} + i\theta_0\right] \tag{10}$$

$$\phi(x, y) = A\exp\left[-\frac{(x^2 + y^2)}{a^2} + \frac{ib(x^2 + y^2)}{2} + i\theta_0\right], \tag{11}$$

where θ_0 is the initial phase of the profile, A is the initial amplitude, a is the width of the beam, and b is the wavefront curvature. The wave function is centered at $(x, y) = (0, 0)$, as shown in Fig. 2.

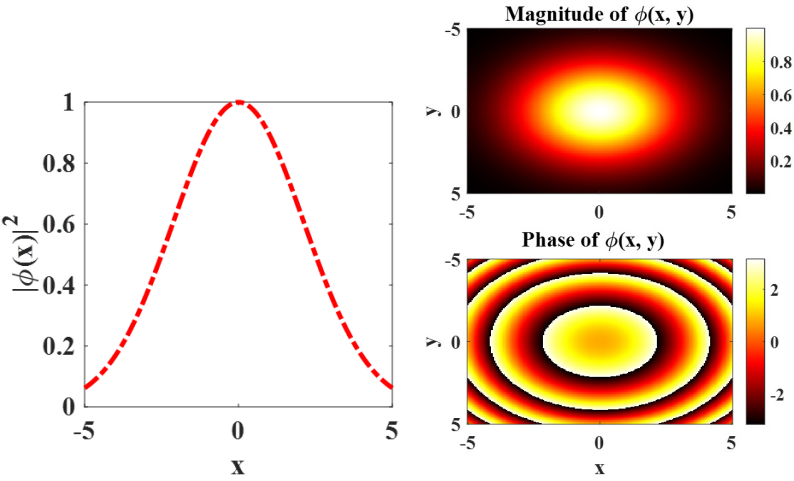

(a) $A = 1$, $a = 2$ and $b = 1$ (b) $A = 1$, $a = 2$ and $b = 1$

Fig. 2. The trial Gaussian solution taken for (a) 1D system (b) 2D system at $A = 1$, $a = 2$ and $b = 1$.

2.1. *Eigenvalues and eigenfunctions of* 1*D beam*

The eigenvalue equation (8) has been numerically analyzed using the finite difference method.[47,48] In this approach, the first- and second-order derivatives of $\phi(x)$ are calculated by expanding the function using Taylor's series and then approximating them with the central difference scheme, following that, an eigenvalue matrix is created. Figures 3(a) and 3(b) depict the imaginary and real components of the eigenvalues corresponding to both the fundamental and excited states of the one-dimensional $\mathcal{PT}$-symmetric cubic system. Similarly, panels (c) and (d) show the eigenvalues for the cubic–quintic system. These eigenvalues are plotted as functions of the imaginary potential coefficient (W) for different values of the cubic nonlinearity (β), specifically at a potential strength of $V_0 = 0.2$ and $\zeta = 0.08$.

For lower values of W, the imaginary component of the eigenvalue, denoted as μ_i, remains at zero, signifying that the eigenvalues are entirely real. This condition implies that the solitons exhibit stability within this specific range. As the value of W increases, μ_i acquires nonzero values, indicating the transition of eigenvalues into the complex plane and suggesting the emergence of instability – a phenomenon characteristic of $\mathcal{PT}$-symmetry breaking.

The value of W where μ_i deviates from zero (highlighted by the labeled markers) delineates the shift from stable to unstable regimes and is known as threshold potential $W_{\rm th}$. It has been shown that $W^1_{\rm th}$ for ground and first overtone is 2.7, 2.1, 1.2 and 0.6 corresponding to $\beta = 0.1, 1, 3$ and 6, respectively, for cubic system and 2.4, 1.5, 0.9 and 0.6, respectively, for cubic–quintic system. Threshold potential $W^2_{\rm th}$ for second and third eigenstates are large when compared with $W^1_{\rm th}$ and they are

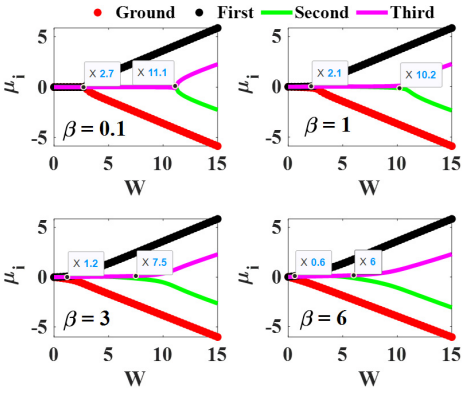

(a) Variation of μ_i of cubic nonlinear system with coefficient of imaginary potential W.

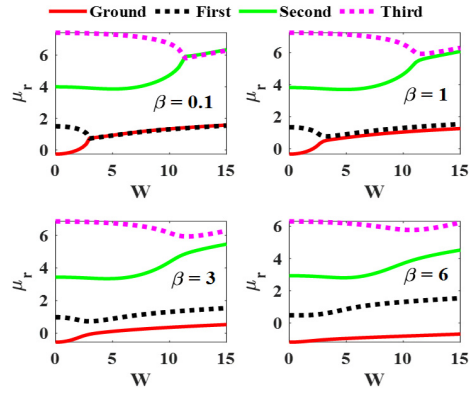

(b) Variation of μ_r of cubic nonlinear system with coefficient of imaginary potential W.

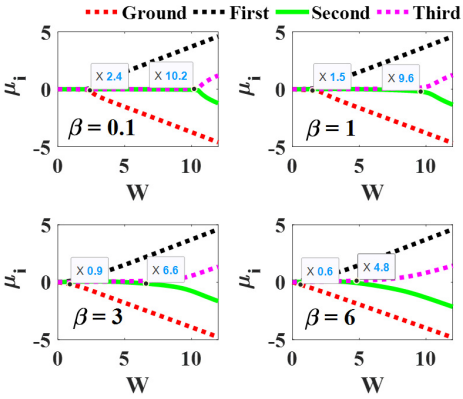

(c) Variation of μ_i of cubic–quintic nonlinear system with coefficient of imaginary potential W.

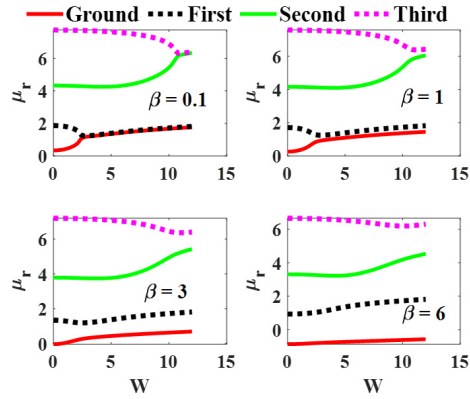

(d) Variation of μ_r of cubic–quintic nonlinear system with coefficient of imaginary potential W.

Fig. 3. Real and imaginary components of eigenvalue of fundamental state and overtones in 1D $\mathcal{PT}$-symmetric system for $\zeta = 0.08$, and $V_0 = 0.2$ (a) Cubic nonlinear system ($\beta_2 = 0$), (b) Cubic–quintic nonlinear system ($\beta_2 = 0.1$).

11.1, 10.2, 7.5 and 6 for the cubic system and 10.2, 9.6, 6.6, and 4.8 for cubic–quintic system.

Larger values of β push the symmetry-breaking point to lower values as indicated in Fig. 3, indicating that stronger nonlinearity cannot maintain $\mathcal{PT}$-symmetric behavior for a longer range, thus destabilizing the beam against the loss/gain caused by the imaginary potential. The periodic nature of both the real and imaginary parts of the potential might support symmetric or anti-symmetric modes. Nonlinearity could selectively stabilize or destabilize these modes depending on their overlap with the gain/loss regions. The behavior of $\mathcal{PT}$-symmetric nonlinear system, particularly

how the instability threshold changes with nonlinearity, is indeed dependent on the specific values of the parameters and coefficients. Different regimes of behavior can emerge depending on the interplay between the depth of the real potential, the strength of the imaginary potential, and the degree of nonlinearity.

The threshold potential W_{th} for the cubic–quintic system is consistently lower than that of the cubic system across all values of β. This suggests that the quintic term amplifies the destabilizing influence of the imaginary potential, as shown in Fig. 4(a). As nonlinearity increases, the system becomes more sensitive to the gain/loss induced by the imaginary part of the potential.

The real potential V_0 in the system generally serves as a confining parameter. The depth of the real potential wells created by $\cos^2(x)$ increases as V_0 rises. As a

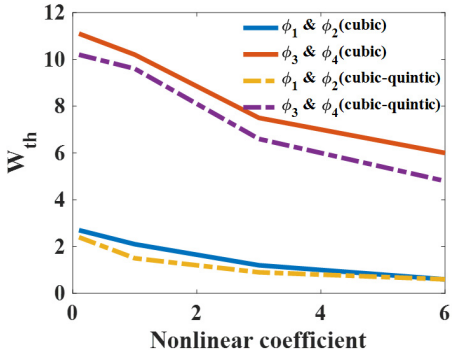

(a) Variation of W_{th} with coefficient of nonlinearity.

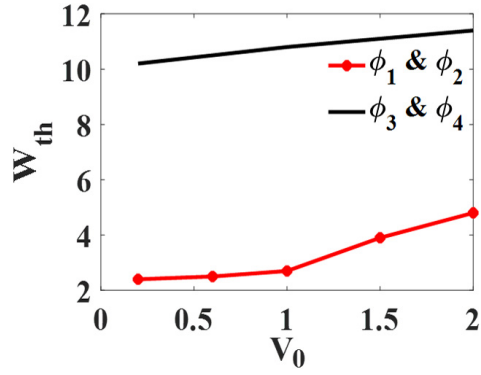

(b) Variation of the threshold potential W_{th} with V_0.

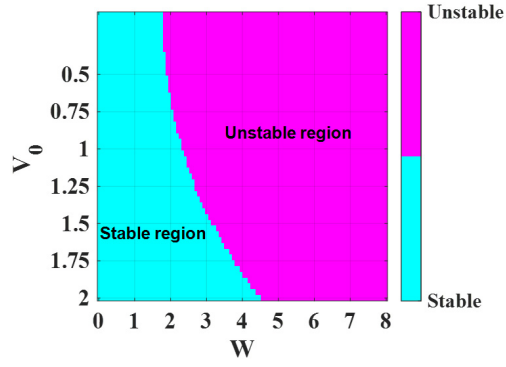

(c) $\zeta = 0.08$, $\beta = 0.1$, and $\beta_2 = 0.1$

Fig. 4. (a) Variation of the threshold potential W_{th} with nonlinear coefficient at $\zeta = 0.08$, and $V_0 = 0.2$ (b) Variation of the threshold potential W_{th} with V_0 at $\beta = 0.1$, $\beta_2 = 0.1$ and $\zeta = 0.08$, (c) Stability regions of solitons in 1D $\mathcal{PT}$-symmetric system in parametric plane of the potential depth (V_0) and the imaginary potential strength (W) at $\zeta = 0.08$, $\beta = 0.1$, and $\beta_2 = 0.1$.

result, within these wells, the wave function becomes more confined. The tendency of wave functions to occupy certain regions more densely as localization grows, the wave function spends less time or has less overlap in the regions where the imaginary potential has a significant effect (both gain and loss). Therefore, the system might become less sensitive to the imaginary potential, and so the threshold for instability increases as shown Fig. 4(b). This is demonstrated in stability chart (Fig. 4(c)) where the boundaries between stable and unstable regions mark the threshold of $\mathcal{PT}$-symmetry breaking.

Figures 5(a) and 5(c) display the ground state and excited state wave profile in $\mathcal{PT}$-symmetric and broken $\mathcal{PT}$-symmetric region. The wave functions have symmetric and confined profiles, and the pattern of peak sequences, such as single, double, triple, and quadruple peaks, for the ground state, first excited state, second excited state, and third excited state indicate a stable system. The eigenfunctions become less localized and asymmetric above the threshold at which the

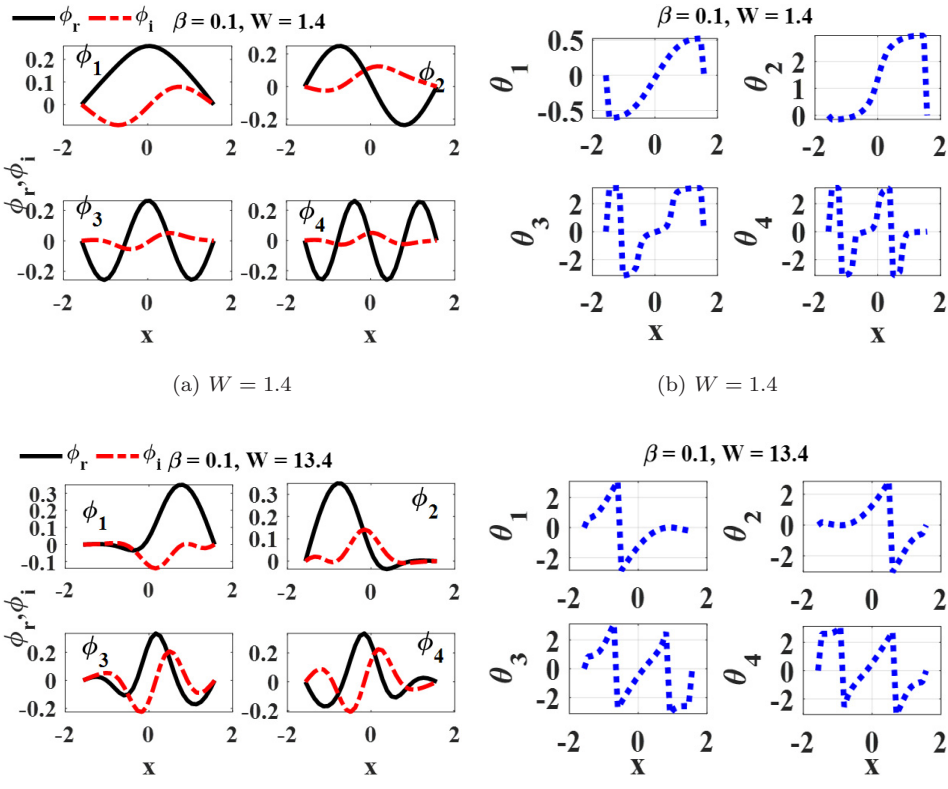

(a) $W = 1.4$ (b) $W = 1.4$

(c) $W = 13.4$ (d) $W = 13.4$

Fig. 5. Eigenfunctions and phases of 1D system in $\mathcal{PT}$-symmetric and broken $\mathcal{PT}$-symmetric regime at $\zeta = 0.08$, $\beta_2 = 0.1$, $\beta = 0.1$ and $V_0 = 0.2$, (a) and (b) $W = 1.4$(Stable), (c) and (d) $W = 13.4$ (unstable), (e) Energy flux versus W at $\beta = 0.1$.

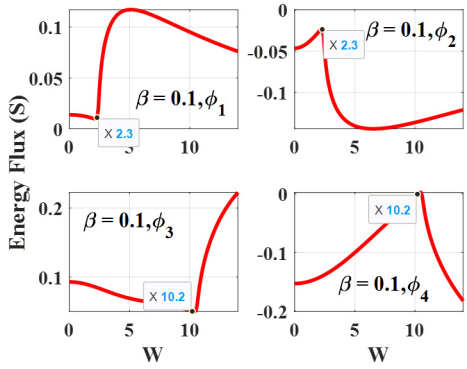

(e) $\beta = 0.1$

Fig. 5. (*Continued*)

$\mathcal{PT}$-symmetry breaks as in Fig. 5(c). This indicates that the system has entered the $\mathcal{PT}-$broken phase, where the solitons or waves may either dissipate or grow uncontrollably.

The phase of these eigenstates is shown in Figs. 5(b) and 5(d), where $\theta = \tan^{-1}(\frac{\phi_i}{\phi_r})$. The imaginary part of the wave function and the phase behavior of the eigenfunctions in $\mathcal{PT}$-symmetric nonlinear systems is closely related. In the $\mathcal{PT}$-symmetric regime, Fig. 5(b), the phase of the eigenfunctions varies smoothly and continuously across the spatial domain. This behavior reflects the symmetry of the eigenfunctions and the real nature of the eigenvalues, signifying the stability of the system and the balance of gain and loss. In contrast, in the broken $\mathcal{PT}$-symmetric regime, Fig. 5(d), the eigenfunctions become asymmetric, and the phase plots exhibit abrupt jumps or discontinuities. These discontinuities correspond to variations in the imaginary part of the eigenfunctions and signal the transition of eigenvalues into the complex plane, marking the onset of instability and $\mathcal{PT}$-symmetry breaking. Moreover, the phases of eigenstates show the complex conjugate behavior of asymmetric eigenfunctions in broken $\mathcal{PT}$-symmetric regime.

Figure 5(e) shows the transverse power flow/Poynting vector of stationary states as a function of W, where

$$S(x) = \frac{i}{2}(\phi\phi_x^* - \phi^*\phi_x).$$

The Poynting vector represents the steady-state allocation of energy flux[49,50] corresponding with each stationary solution rather than the dynamic propagation of energy. Stable soliton propagation results in a steady, positive energy flux. When instability occurs, the Poynting vector can rapidly shift, suggesting variation in energy propagation. When W varies sufficiently, the Poynting vector alters direction and magnitude, indicating the transition from stability to instability. The value of $S(x)$ is either positive or negative depending on the eigenstate, the value of W

and the nonlinear function. The sign and magnitude of S reflect the spatial distribution of energy. All these figures display that, the Poynting vector S exhibits abrupt changes exactly at the threshold potential for every state, indicating a remarkable physical transition or bifurcation point within the system, most likely associated with the stability and existence of the soliton states. The behavior is identical for the ground state and first overtone, whose eigenvalues are complex conjugates, but there is a reversal of energy flow. Negative S suggests complex internal dynamics within the system, such as localized regions where the energy distribution is nonuniform, and potentially leading to complex behaviors like mode switching, or even collapse if the soliton cannot maintain a stable configuration. For higher excited states, also same type of behavior exists after the threshold value which indicates the unstable nature of eigenstates. Thus, significant changes in beam propagation in the $\mathcal{PT}$-symmetric phase and broken $\mathcal{PT}$-symmetric phase are reflected by the energy flux S.

2.2. *Eigenvalues and eigenfunctions of 2D beam evolution*

A 2D $\mathcal{PT}$-symmetric nonlinear system requires spatial modifications across two dimensions, which increases complexity. Parameters like gain, loss, and nonlinear interactions can be adjusted spatially in two directions, resulting in more complex patterns of stability and instability. The interactions of these traits can result in complex spatial structures and influence how solitons or wave patterns form across a plane. This two-dimensionality allows for richer and more diverse spatial phenomena than the one-dimensional situation.

The eigenvalue equation (9) has been numerically analyzed using the finite difference method.[47,48] Figures 6(a) and 6(b) show the imaginary and real parts of

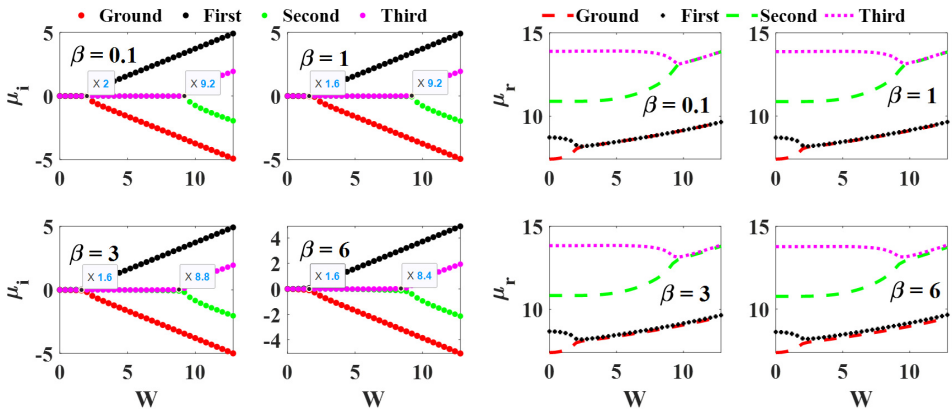

(a) μ_i versus W (b) μ_r versus W

Fig. 6. (a) and (b) Variation of real and imaginary components of eigenvalue of fundamental state and overtones of 2D $\mathcal{PT}$-symmetric system with W for $\zeta = 0.08$, $\beta_2 = 0.1$, and $V_0 = 0.2$.

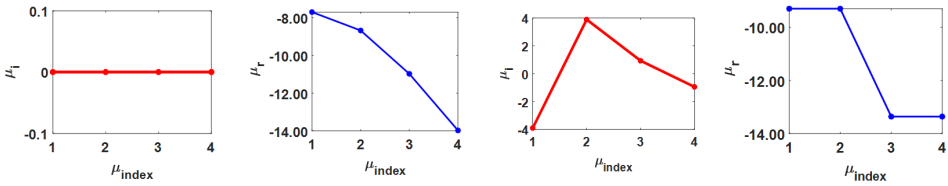

(a) $W = 1.4$ (all states are stable) (b) $W = 13.4$ (all states are unstable)

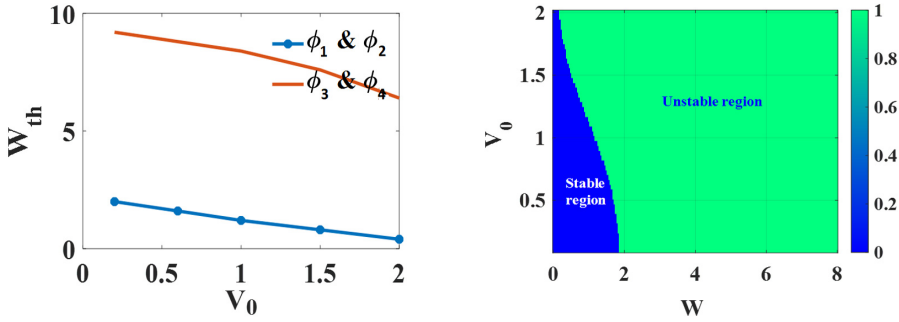

(c) W_{th} versus V_0 (d) W versus V_0

Fig. 7. (a) and (b) Variation of μ_r and μ_i for each eigenstate at $V_0 = 0.2$, $\zeta = 0.08$, $\beta_2 = 0.1$, and $\beta = 0.1$, (c) Variation of the threshold potential W_{th} with the coefficient of real potential (d) Stability regions of solitons in 2D $\mathcal{PT}$-symmetric system in parametric plane of the potential depth (V_0) and the imaginary potential strength (W).

eigenvalues of fundamental and excited states of the 2D $\mathcal{PT}$-symmetric system as function of the imaginary potential coefficient (W) for different values of cubic nonlinearity β at $V_0 = 0.2$, $\zeta = 0.08$, and $\beta_2 = 0.1$. Figures 6 and 7(a) show that for small values of W, all eigenstates are stable and $\mu_i = 0$ (The horizontal axis (μ_{index}) represents the sequential numbering of the eigenmodes (e.g., 1 for the first mode, 2 for the second mode, and so on). But as W goes beyond 2 the first two eigenmodes, and beyond 9.2, second and third eigenmodes become unstable at $\beta = 0.1$. As β increases, the threshold potential decreases as in 1D system.

More spatial modes or channels are available for the light to occupy in a 2D system. These modes may be coupled to one another or generate interference. When paired with the effects of $\mathcal{PT}$-symmetry (gain and loss), the nonlinear interactions between various modes might result in more complex behavior at larger β, potentially leading to instabilities. As this, when the nonlinearity is too strong, it can cause uneven energy exchange between the gain and loss regions, leading to a breakdown of the $\mathcal{PT}$-symmetry.

As an external trapping force, the real potential V_0 reinforces and deepens the confinement of the wave modes. However, in 2D system, the wave function can still interact with a broader range of the potential field because it occupies a region in the xy-plane. So, even small overlaps with the gain or loss regions can have a

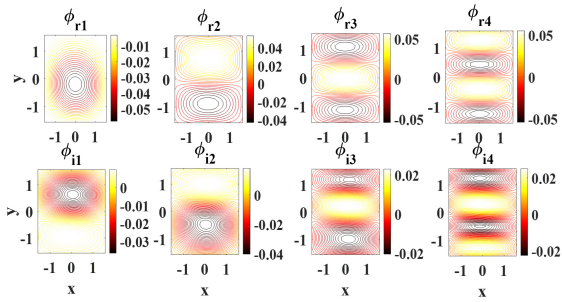

(a) $W = 1.4$ (stable region)

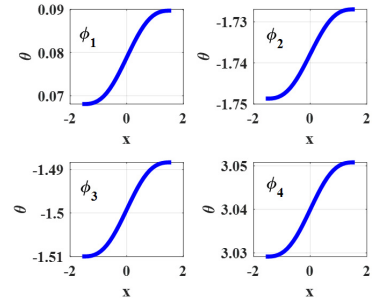

(b) The phase variation of eigenstates at $W = 1.4$

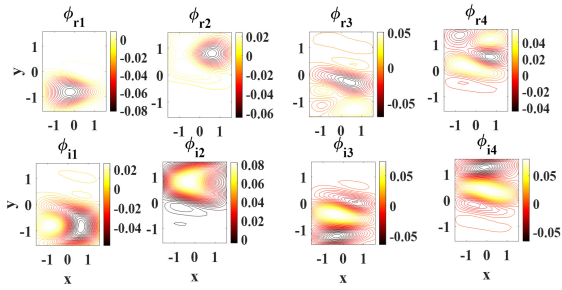

(c) $W = 13.4$ (unstable region)

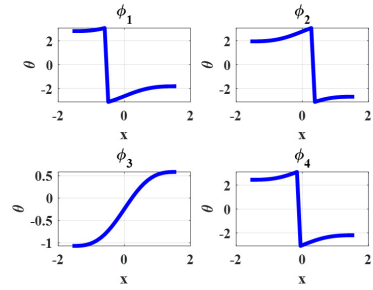

(d) The phase variation of eigenstates at $W = 13.4$

Fig. 8. (a) and (c) The eigenfunctions for each eigenstate in stable and unstable regions at $\zeta = 0.08$, $\beta_2 = \beta = 0.1$, and $V_0 = 0.2$, (b) and (d) Variation of the phase of each eigenstate in stable and unstable regions.

significant impact, leading to rapid amplification or attenuation of certain parts of the wave function which leads to destabilization as V_0 increases as shown in Fig. 7(b). This is demonstrated in stability chart, Fig. 7(d), where the boundaries between stable and unstable regions mark the threshold of $\mathcal{PT}$-symmetry breaking.

Figure 8(a) shows the eigenfunction representing beam in 2D $\mathcal{PT}$-symmetric system below the threshold potential. In the stable region, the real and imaginary components of the eigenfunctions exhibit symmetry, indicating that the optical field remains well-constrained and experiences minimal distortion during propagation. Here the gain and loss regions are balanced so that energy does not flow excessively in or out of any particular region. In addition, the symmetry suggests that the mode is localized, which is indicative of stability in such systems because it is neither rapidly growing nor sinking. In contrast, Fig. 8(c) is the 2D eigenfunction of the system in the broken $\mathcal{PT}$-symmetric region, which are asymmetric and unlocalized. This suggests the unstable nature of the eigenmode above the threshold potential.

Figure 8(b) demonstrates that there are no sharp discontinuities or jumps in the optical field's phase as it varies gradually along the wave function. This smooth

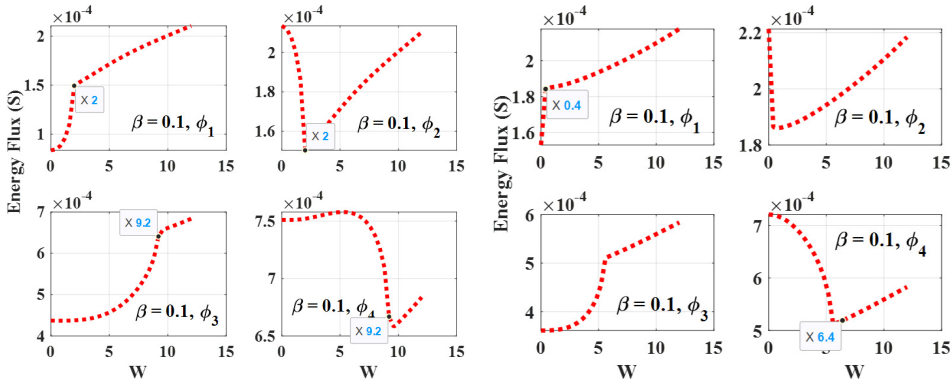

(a) $V_0 = 0.2$ (b) $V_0 = 2$

Fig. 9. Variation of the energy flux (Poynting vector) with W for each eigenstate at $\zeta = 0.08$, $\beta_2 = \beta = 0.1$.

change is indicative of a stable propagation mode, in which there are no notable disturbances that could quickly produce phase shifts in the beam. Phase leaps prevent abrupt changes in the direction of energy flow, which aids in preserving the beam's integrity during propagation. However, these types of behaviors cannot be seen in the broken $\mathcal{PT}$-symmetric region, where phase changes of eigenmodes occur abruptly and discontinuously as in Fig. 8(d).

Figure 9 represents the energy flux associated with 2D $\mathcal{PT}$-symmetric system which shows the stability and instability of eigenstates within $\mathcal{PT}-$ symmetric and broken $\mathcal{PT}-$ symmetric phases.[51] For all eigenstates, the system may discontinuously go to a shift at W_{th} which indicates the instability of the state. The behavior is identical for the ground state (ϕ_1) and first overtone (ϕ_2), whose eigenvalues are complex conjugates, but there is a phase reversal of energy flow for ϕ_2. In the cases of higher excited states, as W surpasses the critical values, the energy flow is reversed for ϕ_4. The system shows the irregular behavior of eigenmodes, signaling that the $\mathcal{PT}$-symmetry is breaking down, and the modes are no longer stable.

Figure 10 demonstrates the intensity distribution of stationary eigenstates below and above the breaking point. The intensity distribution of ϕ_1 shows a single peak at the center, which indicates a fundamental soliton. The peak is symmetric about $(x, y) = (0, 0)$ and well-localized, characteristic of stable solitons in the $\mathcal{PT}$-symmetric system below the threshold. The intensity distribution of ϕ_2, ϕ_3 and ϕ_4 are more complex than the fundamental state and characterized by multiple peaks. Here the energy is dispersed over more spatial regions, characteristic of higher-order modes in nonlinear systems. However, the energy or intensity of all states is constant, irrespective of the order of state. Above the threshold potential, the distribution of all states shows asymmetry and has slightly higher amplitudes. The pattern of multi-peaks might become less distinct or more diffuse by losing its regular pattern, suggesting the loss of symmetry and stability.

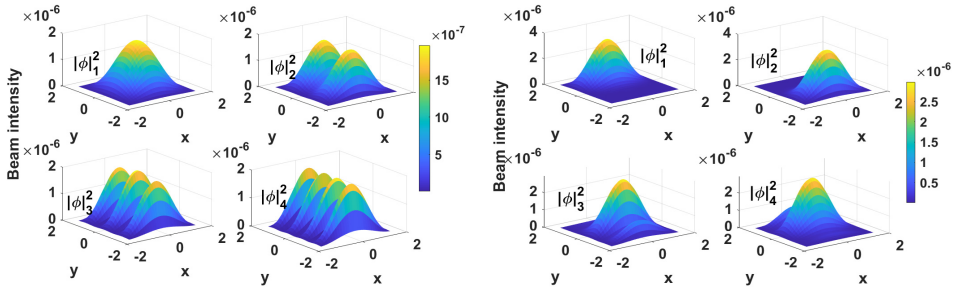

(a) $W = 1.4$ (b) $W = 13.4$

Fig. 10. Intensity of nonlinear $\mathcal{PT}$-symmetric stationary eigenstates in focusing system for $\beta_2 = \beta = 0.1$, $\zeta = 0.08$ (a) $W = 1.4$ (b) $W = 13.4$ while W_{th}^1 is 2 and W_{th}^2 is 9.2.

3. Stability of 1D and 2D Optical Beams

One defining characteristic of optical solitons is their exceptional ability to resist perturbations. This innate stability enables them to maintain their shape and dynamics. In the context of $\mathcal{PT}$-symmetric potentials, we explore deeper into this stability by analyzing how these solitary waves react to perturbations. The goal here is to understand how stationary and centrally symmetric solitons, which are initially stable, respond to disturbances of the same dimension that do not disrupt their symmetry. The stability of the stationary solution of 1D system was investigated by applying the following perturbation:

$$\psi(x,z) = [\phi(x) + g(x,z)]\exp[-i\mu z]. \tag{12}$$

$$g(x,z) = p(x)e^{i\lambda z} + q(x)e^{-i\lambda^* z}, \tag{13}$$

where $p(x)$ and $q(x)$ are perturbing functions with $|p(x)|, |q(x)| \ll \phi(x)$. By applying this solution into Eq. (1) and linearizing, we get Bogoliubov–de Gennes (BDG) equations in matrix form as

$$\lambda \begin{bmatrix} p \\ q^* \end{bmatrix} = \begin{bmatrix} L_1 & L_2 \\ L_2^* & -L_1^* \end{bmatrix} \begin{bmatrix} p \\ q^* \end{bmatrix}. \tag{14}$$

$$L_1 = \zeta \frac{d^2}{dx^2} + V(x) + \mu + 2\beta|\phi(x)|^2 + 3\beta_2|\phi(x)|^4, \tag{15}$$

$$L_2 = \beta\phi(x)^2 + 2\beta_2\phi(x)^2|\phi(x)|^2. \tag{16}$$

One distinguishing feature of these systems is that the eigenvalues λ appear in complex conjugate pairs. This means that both λ and its complex conjugate, λ^* are eigenvalues simultaneously. This characteristic results directly from the nonlinear optical structure's inherent $\mathcal{PT}$-symmetry. Figure 11 shows the stability spectrum of the 1D beam in $\mathcal{PT}$-symmetric system under perturbation. For $W = 1.4$ (below the threshold), the imaginary part of perturbed eigenvalues λ_i is zero and eigenfunctions

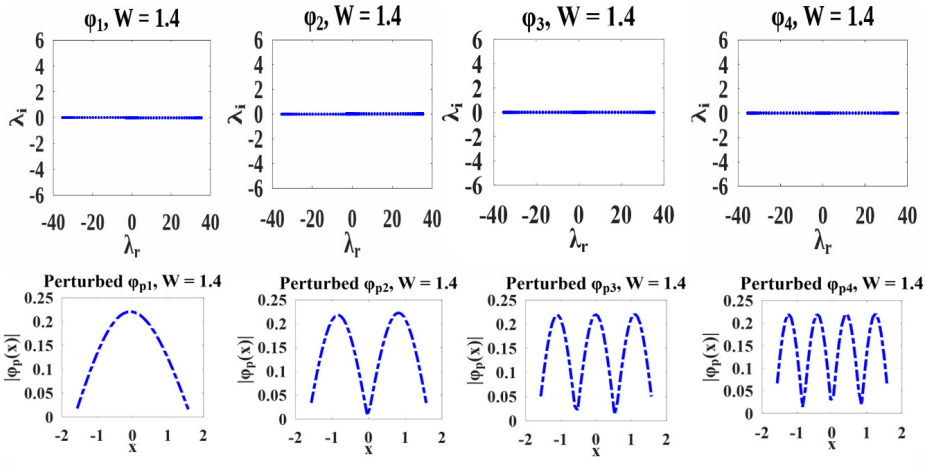

(a) $W = 1.4$

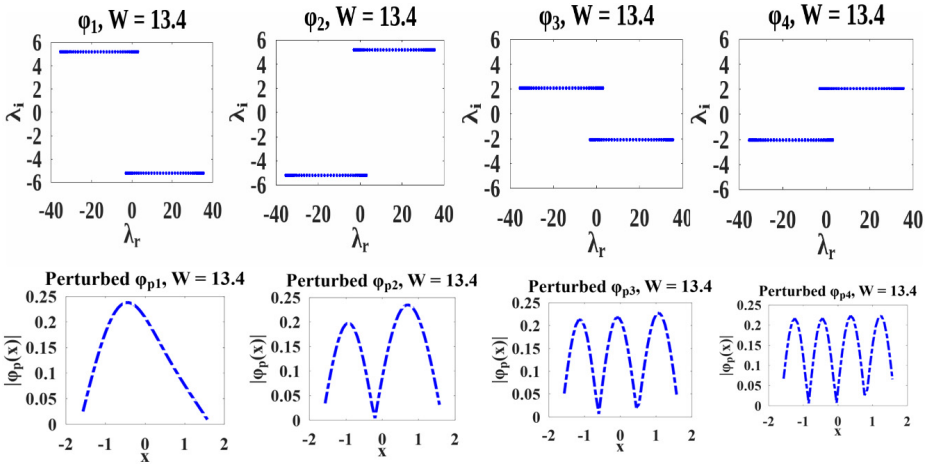

(b) $W = 13.4$

Fig. 11. Perturbed eigenvalues and eigenfunctions (1D) below and above the threshold potential at $\beta_2 = \beta = 0.1$, $V_0 = 0.2$, and $\zeta = 0.08$.

(perturbed eigenfunctions ϕ_p) are symmetric about $x = 0$, indicating that the solution is stable and not oscillatory. For $W = 13.4$, all states are unstable and the imaginary parts are nonzero for all eigenmodes and eigenfunctions are asymmetric.

The stability of the stationary solution of 2D system was investigated by applying the following perturbation:

$$\psi(x, y, z) = [\phi(x, y) + g(x, y, z)]\exp[-i\mu z], \tag{17}$$

$$g(x, y, z) = p(x, y)e^{i\lambda z} + q(x, y)e^{-i\lambda^* z}, \tag{18}$$

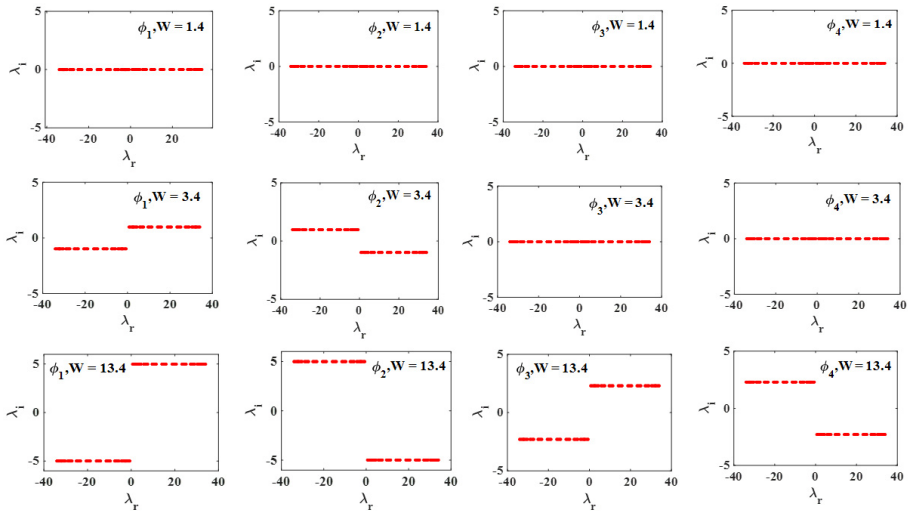

Fig. 12. Real and imaginary components of perturbed eigenvalue at $\beta_2 = \beta = 0.1$, $V_0 = 0.2$, and $\zeta = 0.08$.

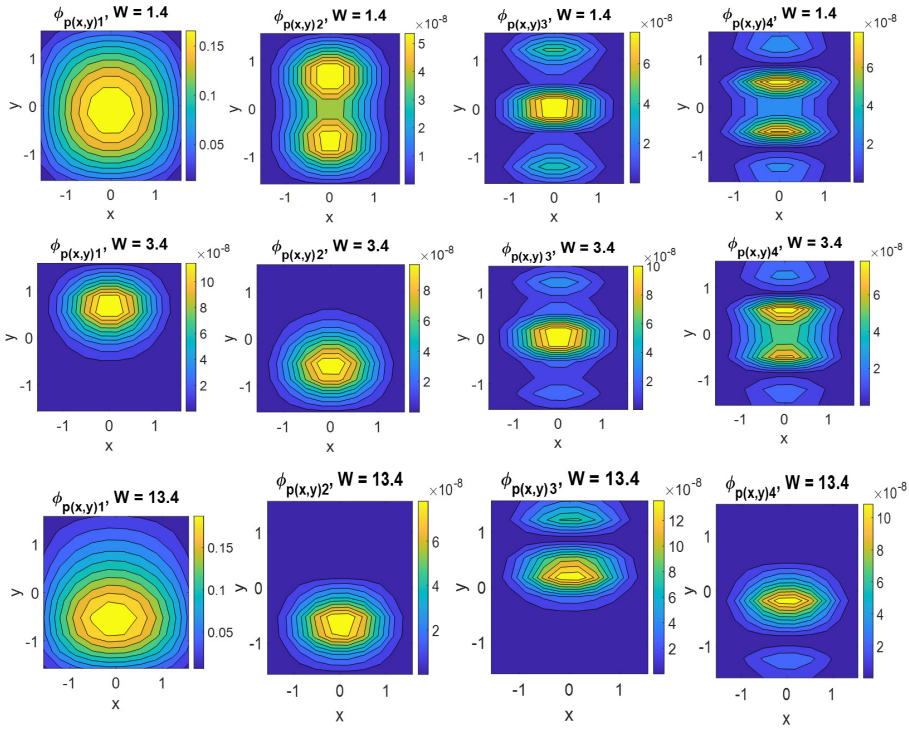

Fig. 13. Perturbed eigenfunctions below and above the threshold potential at $\beta_2 = \beta = 0.1$, $V_0 = 0.2$, and $\zeta = 0.08$.

where $p(x, y)$ and $q(x, y)$ are perturbing functions with $|p(x, y)|, |q(x, y)| \ll \phi(x, y)$. By applying this solution into Eq. (2) and linearizing, we get BDG equations in matrix form as Eq. (14), where

$$L_1 = \zeta \left(\frac{d^2}{dx^2} + \frac{d^2}{dy^2} \right) + V(x, y) + \mu + 2\beta|\phi(x, y)|^2 + 3\beta_2|\phi(x, y)|^4, \tag{19}$$

$$L_2 = \beta\phi(x, y)^2 + 2\beta_2\phi(x, y)^2|\phi(x, y)|^2. \tag{20}$$

Figures 12 and 13 show the stability spectrum and perturbed eigenfunctions $\phi_p(x, y))$ of the 2D beam in $\mathcal{PT}$-symmetric system under perturbation. As in 1D, below the instability threshold, the eigenmodes are localized, and their energy is concentrated abut $x = y = 0$, leading to stable and non-oscillatory behavior. When W exceeds the threshold, the system enters the broken $\mathcal{PT}$-symmetric regime, where eigenmodes corresponding to nonzero imaginary eigenvalues dominate. This breaking of symmetry results in the distorted and asymmetric shapes of the eigenfunctions, and it corresponds to energy imbalance in the system. For $W = 3.4$, the second eigenstates and third eigenstates are stable, while the first two modes appear distorted and asymmetric. For $W = 13.4$, all eigenstates are going to be unstable and all eigenstates are subject to exponential growth, leading to a breakdown of the localized structures.

4. Threshold Effects on Beam Propagation in 1D and 2D Nonlinear $\mathcal{PT}$-Symmetric Media

The wave patterns which describe the propagation of the stationary solution of Eqs. (1) and 2 are established using the finite difference beam propagation method which allows simulation of beam transmission in 1D and 2D $\mathcal{PT}$-symmetric systems. The Crank–Nicolson technique[47,48,52–56] is used to discretize NLSE and convert it into a difference equation on a rectangular grid. This grid is defined by spacing Δz along the propagation direction and Δx and Δy along the transverse dimensions, where $z_j = j\Delta z$, $y_m = m\Delta y$ and $x_n = n\Delta x$. For 1D system, the method ensures stability as long as $\frac{\Delta z}{(\Delta x)^2} \leq 0.5$. Let ψ_j^n denote the wave pattern at the grid point (j, n) and ψ_j^{n+1} generated by the matrix $A_x\psi_j^{n+1} = B_x\psi_j^n$, where A_x and B_x, stand for tridiagonal matrices corresponding to the discretization in the x direction. For 2D system, the condition for stability of the method is $\frac{\Delta z}{(\Delta x)^2} + \frac{\Delta z}{(\Delta y)^2} \leq 0.5$. Let $\psi_j^{n,m}$ denote the wave pattern at the grid point (j, n, m) and $\psi_j^{n+1,m}$ and $\psi_j^{n,m+1}$ generated by the matrix $A_x\psi_j^{n+1,m} = B_x\psi_j^{n,m}$ and $A_y\psi_j^{n,m+1} = B_y\psi_j^{n,m}$, where A_x, B_x, A_y and B_y stand for tridiagonal matrices corresponding to the discretization in the x and y directions. The trial solution for the system in 1D is

$$\phi(x, z) = A(z) \exp\left(\frac{-x^2}{a(z)^2} + \frac{ib(z)x^2}{2} + i\theta_0 \right) \tag{21}$$

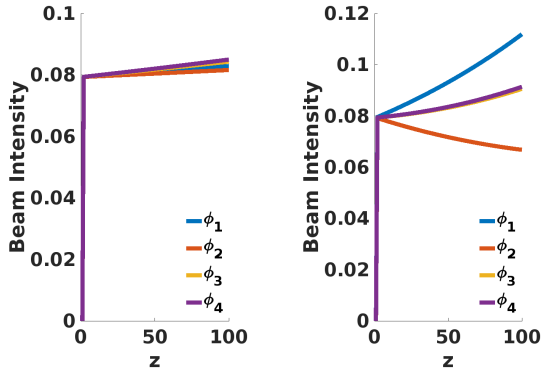

(a) $W = 1.4$ (b) $W = 13.4$

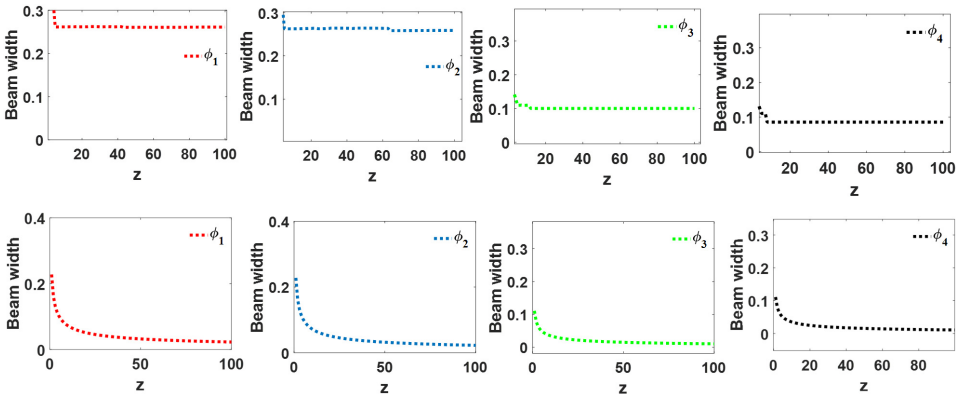

(c) First row: $W = 1.4$, Second row: $W = 13.4$

Fig. 14. Intensity of nonlinear $\mathcal{PT}$-symmetric stationary eigenstates in 1D focusing system for $\beta_2 = \beta = 0.1$, $\zeta = 0.08$ (a) $W = 1.4$ (b) $W = 13.4$, (c) Variation of the beam width below and above the threshold potential.

and for 2D the trial solution is

$$\phi(x, y, z) = A(z) \exp\left(\frac{-(x^2 + y^2)}{a(z)^2} + \frac{ib(z)(x^2 + y^2)}{2} + i\theta_0\right). \tag{22}$$

The beam amplitude, intensity, and beam width of the optical wave during propagation have been established in $\mathcal{PT}$-symmetric and broken $\mathcal{PT}$-symmetric regions. Figures 14(a) and 14(b) represent the intensity of the beam as function of the propagation distance below and above the threshold potential. For $W = 1.4$, the beam intensity does not vary significantly during the propagation, indicating that propagation is stable. But when the potential goes beyond the threshold, the beam intensity varies. Figure 14(c) shows how the beam's (or wave packet's) width changes along the propagation direction. The width of the beam remains constant throughout the propagation when the system is in $\mathcal{PT}$-symmetric regime. However,

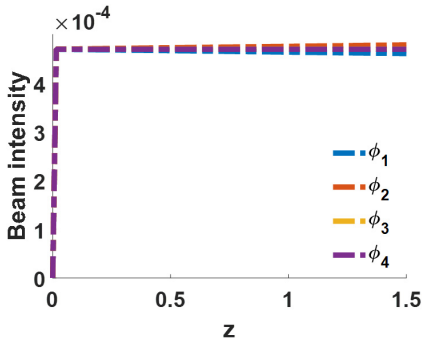

(a) $W = 1.4$

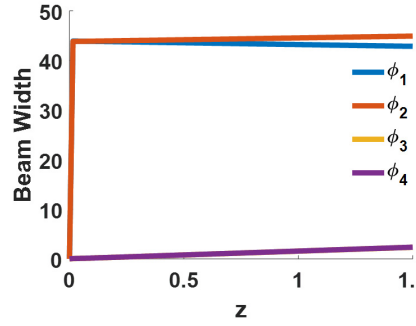

(b) $W = 1.4$

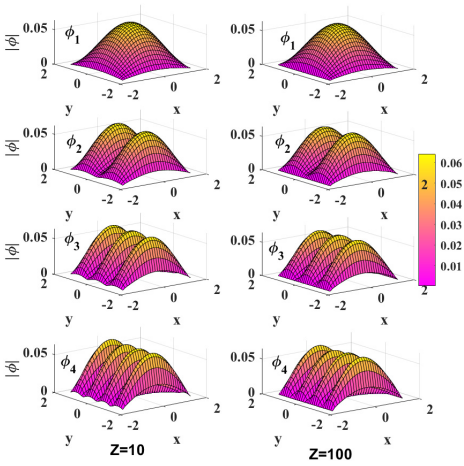

(c) $W = 1.4$

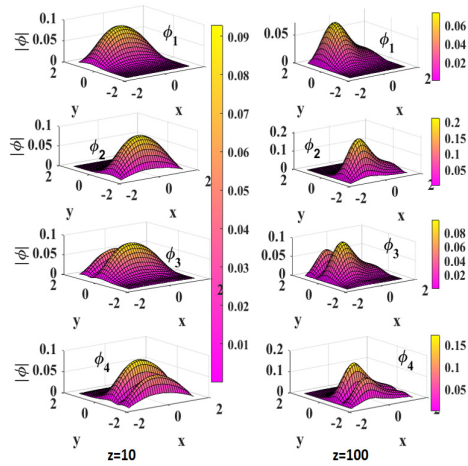

(d) $W = 13.4$

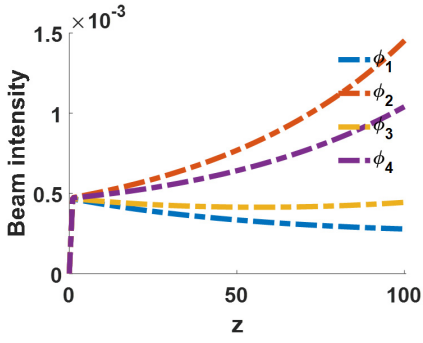

(e) $W = 13.4$

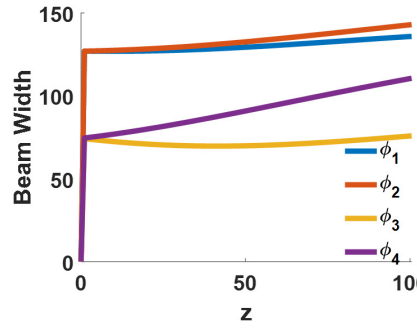

(f) $W = 13.4$

Fig. 15. At $\beta_2 = \beta = 0.1$, $\zeta = 0.08$ (a)–(c) Variation of the power, the width and the waveform of eigenstates during propagation in the stable region, (d)–(f) The asymmetrical waveform, the power and beam width of the wave during propagation in the unstable region.

nonlinearity and the complex potential's influence can be combined to provide the compression of the beam when the system is nonlinear and the field is above the breaking potential. The system may be strongly focusing the beam during the first propagation phase, as indicated by the rapid initial fall in width.

Figures 15(a) and 15(b) represent the beam intensity and width as functions of propagation distance z for 2D system. The beam width does not fluctuate much across the propagation distance for $W = 1.4$ and the beam intensity stays relatively constant, showing a steady propagation for $W = 1.4$. This stability indicates that the system is in the $\mathcal{PT}$-symmetric phase of gain and loss balance, which permits continuous wave propagation without collapse or divergence. Figure 15(c) depicts the spatial distribution of the beam (perhaps as a function of x and y) at various propagation distances. The beam does not exhibit any diffraction or nonlinearity-induced effects, which would normally result in spreading or focusing, and the peak intensity stays centered. The beam's stability in the $\mathcal{PT}$-symmetric phase is confirmed by its consistent shape and size across different z values.

The profiles of the beam at various propagation distances are shown in Fig. 15(d) for $W = 13.4$. The profiles in this broken $\mathcal{PT}$-symmetric phase are probably quite variable, exhibiting deformation, peak intensity variations, and broadening, all of which point to instability. Here, the gain and loss are no longer balanced, leading to exponential growth or decay of the beam's amplitude, depending on the propagation distance, as shown in Figs. 15(e) and 15(f). The intensity of ϕ_1 and ϕ_3 decreases while that of ϕ_2 and ϕ_4 increases. It is because ϕ_1 and ϕ_3 have eigenvalues that have negative imaginary part, while ϕ_2 and ϕ_4 have positive imaginary part.

5. Conclusion

This work explores the evolution of nonlinear eigenmodes in $\mathcal{PT}$-symmetric 1D and 2D sinusoidal systems. We examined an optical system with a complex potential that permits real eigenvalue spectra up to a critical potential known as the symmetry-breaking point. By using numerical methods, we analyzed both fundamental and higher-order eigenmodes. Our findings indicate that the threshold potential decreases with increasing the nonlinearity and increases with the depth of the real component of the potential in 1D systems. The threshold potential Wth for the cubic–quintic system is consistently lower than that of the cubic system across all values of cubic nonlinearity. This suggests that the quintic term amplifies the destabilizing influence of the imaginary potential. As nonlinearity increases, the system becomes more sensitive to the gain/loss induced by the imaginary part of the potential. We developed eigenfunctions, that demonstrate the symmetric behavior below this imaginary threshold potential. These eigenfunctions exhibit a regular sequence in the number of peaks, and the energy flux shows no abrupt jumps. The phase of each eigenstate varies smoothly in accordance with the imaginary part of the eigenfunction along the wave function. In the broken $\mathcal{PT}$-symmetric phase, the eigenfunctions become asymmetric about $x = 0$, signaling instability of the beam.

This instability manifests as a sudden shift in the energy flux at the threshold, and the phases of eigenstates reflect the complex conjugate behavior of the asymmetric eigenfunctions.

The stability analysis has been performed using BDG matrix method and established that the eigenstates are stable below the threshold potential even in the presence of small perturbation but loses stability when the potential crosses the limit.

The investigation was extended to a $\mathcal{PT}$-symmetric 2D system, where the beam is spatially localized within a plane and supported by a 2D $\mathcal{PT}$-symmetric potential field. Analogous to the 1D case, the stability of eigenmodes in this 2D system diminishes with increasing nonlinearity but is enhanced by the depth of the real potential. Here, the real potential V_0 acts as an external trapping force, strengthening and deepening the confinement of the wave modes. However, in a 2D system, the wave function interacts with a broader range of the potential field, as it spans an extended region in the xy-plane. Consequently, even minor overlaps with gain or loss regions can significantly affect the wave function, leading to rapid amplification or attenuation in localized regions, which contributes to destabilization as V_0 increases.

Below the threshold limit, stationary eigenfunctions exhibit central symmetry and show smooth phase variations. Above this threshold, however, symmetry is lost, and the eigenfunctions become asymmetric. The behavior of the energy flux reflects the stability of the beam: the energy or intensity remains constant across all states regardless of their order. Beyond the threshold potential, the distribution of eigenstates becomes asymmetric and exhibits slightly increased amplitudes. The multi-peak patterns may become less distinct or more diffuse, indicating a loss of symmetry and stability.

A stability analysis of the 2D system was performed, yielding conditions for more precisely defined thresholds, enhanced damping of perturbation-induced growth that destabilizes eigenmodes, and advanced mechanisms for managing perturbations and potential interactions.

The propagation dynamics of stationary eigenmodes were also examined for both 1D and 2D systems, demonstrating that amplitude and beam width remain constant in the $\mathcal{PT}$-symmetric phase, while they decrease or increase in the broken $\mathcal{PT}$-symmetric phase.

Our conclusions sound very interesting and present viable approaches for controlling and stabilizing beam propagation in optical system using $\mathcal{PT}$-symmetric potentials in a range of parameter domains. Development of reliable optical communication channels can be aided by understanding the stability and eigenmode behavior of 1D $\mathcal{PT}$-symmetric systems. One can create optical fibers or waveguides that are resistant to flaws and losses, improving signal integrity and transmission efficiency, by taking advantage of the capacity to maintain real eigenvalue spectra despite complex potentials. By modifying the symmetry and stability of eigenmodes, lasers with distinct emission patterns and decreased sensitivity to disturbances can be produced, potentially enhancing beam quality and coherence.

The study of eigenmode stability and phase variations can be utilized in the development of high-precision sensors in detecting small changes in external conditions.

Imaging technologies can benefit from the management of beam localization and stability in 2D $\mathcal{PT}$-symmetric systems. The insights acquired from studying how eigenmodes interact with potential fields might help to improve imaging systems by allowing for greater control over image resolution and quality, especially in complicated contexts. The ability to control beam shapes and patterns in 2D systems is useful for applications like optical trapping and beam steering, where more complex beam profiles are needed.

ORCID

C. P. Jaseera https://orcid.org/0009-0007-9299-1612
K. Aysha Muhsina https://orcid.org/0000-0003-4114-699X

References

1. R. El-Ganainy, K. G. Makris, D. N. Christodoulides and Z. H. Musslimani, Theory of coupled optical pt-symmetric structures, *Opt. Lett.* **32** (2007) 2632–2634, https://opg.optica.org/ol/abstract.cfm?URI=ol-32-17-2632.
2. C. M. Bender and S. Boettcher, Real spectra in non-Hermitian Hamiltonians having $\mathcal{PT}$-symmetry, *Phys. Rev. Lett.* **80** (1998) 5243, https://link.aps.org/doi/10.1103/PhysRevLett.80.5243.
3. C. M. Bender, D. C. Brody and H. F. Jones, Complex extension of quantum mechanics, *Phys. Rev. Lett.* **89** (2002) 270401, https://link.aps.org/doi/10.1103/PhysRevLett.89.270401.
4. C. M. Bender, Introduction to $\mathcal{PT}$-symmetric quantum theory, *Contemp. Phys.* **46** (2005) 277–292, https://doi.org/10.1080/00107500072632.
5. C. Ruter, K. Makris and R. El Ganainy *et al.*, Observation of parity-time symmetry in optics, *Nat. Phys.* **6** (2010) 192–195, https://doi.org/10.1038/nphys1515.
6. A. Guo, G. J. Salamo, D. Duchesne, R. Morandotti, M. Volatier-Ravat, V. Aimez, G. A. Siviloglou and D. N. Christodoulides, Observation of $\mathcal{PT}$-symmetry breaking in complex optical potentials, *Phys. Rev. Lett.* **103** (2009) 093902, https://link.aps.org/doi/10.1103/PhysRevLett.103.093902.
7. O. Bendix, R. Fleischmann, T. Kottos and B. Shapiro, Exponentially fragile $\mathcal{PT}$-symmetry in lattices with localized eigenmodes, *Phys. Rev. Lett.* **103** (2009) 030402, https://link.aps.org/doi/10.1103/PhysRevLett.103.030402.
8. S. Klaiman, U. Günther and N. Moiseyev, Visualization of branch points in $\mathcal{PT}$-symmetric waveguides, *Phys. Rev. Lett.* **101** (2008) 080402, https://link.aps.org/doi/10.1103/PhysRevLett.101.080402.
9. T. Kottos, Broken symmetry makes light work, *Nat. Phys.* **6** (2010) 166–167, https://doi.org/10.1038/nphys1612.
10. S. Longhi, Bloch oscillations in complex crystals with $\mathcal{PT}$-symmetry, *Phys. Rev. Lett.* **103** (2009) 123601, https://link.aps.org/doi/10.1103/PhysRevLett.103.123601.
11. Z. H. Musslimani, K. G. Makris, R. El-Ganainy and D. N. Christodoulides, Optical solitons in $\mathcal{PT}$-periodic potentials, *Phys. Rev. Lett.* **100** (2008) 030402, https://link.aps.org/doi/10.1103/PhysRevLett.100.030402.

12. A. Regensburger, C. Bersch, M. A. Miri, D. N. C. G. Onishchukov and U. Peschel, Parity-time synthetic photonic lattices, *Nature* **488** (2012) 167–171, https://doi.org/10.1038/nature11298.
13. N. Lazarides and G. P. Tsironis, Gain-driven discrete breathers in $\mathcal{PT}$-symmetric nonlinear metamaterials, *Phys. Rev. Lett.* **110** (2013) 053901, https://link.aps.org/doi/10.1103/PhysRevLett.110.053901.
14. K. Aysha Muhsina and P. A. Subha, Spatial solitons in a medium with lumped amplification and dissipation, *J. Nonlinear Opt. Phys. Mater.* **24** (2015) 1550011, https://doi.org/10.1142/S0218863515500113.
15. M. Segev, Optical spatial solitons, *Chaos* **10** (1998) 603–612, http://doi.org/10.1023/A:1006915021865.
16. A. T. Avelar, D. Bazeia and W. B. Cardoso, Solitons with cubic and quintic nonlinearities modulated in space and time, *Phys. Rev. E* **79** (2009) 025602, https://link.aps.org/doi/10.1103/PhysRevE.79.025602.
17. D. Mihalache, D. Mazilu, Crasovan, B. A. Malomed, F. Lederer and L. Torner, Robust soliton clusters in media with competing cubic and quintic nonlinearities, *Phys. Rev. E* **68** (2003) 046612, https://link.aps.org/doi/10.1103/PhysRevE.68.046612.
18. M. Aleksandra, H. Ljup and M. Boris, Dark solitons in dynamical lattices with the cubic-quintic nonlinearity, *Phys. Rev. E* **76** (2007) 046605, https://link.aps.org/doi/10.1103/PhysRevE.76.046605.
19. C. Mejía-Cortés, R. A. Vicencio and B. A. Malomed, Mobility of solitons in one-dimensional lattices with the cubic-quintic nonlinearity, *Phys. Rev. E* **88** (2013) (2013) 052901, https://link.aps.org/doi/10.1103/PhysRevE.88.052901.
20. W. Chen, M. Shen, Q. Kong, J. Shi, Q. Wang and W. Krolikowski, Interactions of nonlocal dark solitons under competing cubic–quintic nonlinearities, *Opt. Lett.* **39** (2014) 1764–1767, https://opg.optica.org/ol/abstract.cfm?URI=ol-39-7-1764.
21. G. Burlak and B. A. Malomed, Stability boundary and collisions of two-dimensional solitons in $\mathcal{PT}$-symmetric couplers with the cubic-quintic nonlinearity, *Phys. Rev. E* **88** (2013) 062904, https://link.aps.org/doi/10.1103/PhysRevE.88.062904.
22. S. Liu, C. Ma, Y. Zhang and K. Lu, Bragg gap solitons in $\mathcal{PT}$-symmetric lattices with competing nonlinearity, *Opt. Commun.* **285** (2012) 1934–1940, https://doi.org/10.1016/j.optcom.2011.11.065.
23. A. Khare, S.M.Al-Marzoug and H. Bahlouli, Solitons in $\mathcal{PT}$-symmetric potential with competing nonlinearity, *Phys. Lett. A* **376** (2012) 2880–2883, https://doi.org/10.1016/j.physleta.2012.09.047.
24. B. Midya and R. Roychoudhury, Nonlinear localized modes in $\mathcal{PT}$-symmetric rosen-morse potential wells, *Phys. Rev. A* **87** (2013) 045803, https://link.aps.org/doi/10.1103/PhysRevA.87.045803.
25. K. G. Makris, R. El-Ganainy, D. N. Christodoulides and Z. H. Musslimani, Beam dynamics in $\mathcal{PT}$-symmetric optical lattices, *Phys. Rev. Lett.* **100** (2008) 103904, https://link.aps.org/doi/10.1103/PhysRevLett.100.103904.
26. V. V. Konotop, J. Yang and D. A. Zezyulin, Nonlinear waves in $\mathcal{PT}$-symmetric systems, *Rev. Mod. Phys.* **88** (2016) 035002, https://link.aps.org/doi/10.1103/ RevModPhys.88.035002.
27. I. V. Barashenkov, D. A. Zezyulin and V. V. Konotop, Jamming anomaly in $\mathcal{PT}$-symmetric systems, *New J. Phys.* **18** (2016) 075015, https://dx.doi.org/10.1088/1367-2630/18/7/075015.
28. D. A. Zezyulin and V. V. Konotop, Nonlinear modes in the harmonic $\mathcal{PT}$-symmetric potential, *Phys. Rev. A* **85** (2012) 075015, https://link.aps.org/doi/10.1103/PhysRevA.85.043840.

29. A. R. Thasneem and P. A. Subha, One-dimensional pt-symmetric eigenmodes in k-wave number Scarf ii potential with defocusing nonlinearity, *Phys. Scr.* **98** (2023) 045203, https://dx.doi.org/10.1088/1402-4896/acb32a.
30. A. R. Thasneem and P. A. Subha, Stationary states and switching dynamics of the self-defocusing nonlinear coupled system with pt-symmetric k-wavenumber Scarf ii potential, *Chaos Solitons Fractals* **172** (2023) 113620, https://www.sciencedirect.com/science/article/pii/S0960077923011475.
31. A. R. Thasneem, P. A. Subha and K. Aysha Muhsina, Stationary states of parity-time symmetric dark solitons in super-Gaussian potential, *Optik* **272** (2022) 170202, https://www.sciencedirect.com/science/article/pii/S0030402622008294.
32. A. R. Thasneem and P. A. Subha, Self-defocusing nonlinear coupled system with PT-symmetric super-Gaussian potential, *Chaos* **33** (2023) 083118, https://doi.org/10.1063/5.0159925.
33. C. P. Jaseera, K. A. Muhsina and A. R. Thasneem, Nonlinear eigen modes in optical media supported by cubic and quintic nonlinearities with parity-time symmetric hyperbolic complex potential, *Optik* **311** (2024) 171899, https://doi.org/10.1016/j.ijleo.2024.171899.
34. C. P. Jaseera, K. A. Muhsina and A. R. Thasneem, Stability of bright solitons in optical system supported by cubic and quintic nonlinearities with $\mathcal{PT}$-symmetric quartic harmonic complex potential, *Phys. Scr.* **99** (2024) 085266, https://dx.doi.org/10.1088/1402-4896/ad6537.
35. C. P. Jaseera, K. A. Muhsina and A. R. Thasneem, Beam propagation in cubic-quintic nonlinear optical system supported by modified parity-time symmetric Rosen–Morse complex potential, *Chaos* **34** (2024) 073139, https://doi.org/10.1063/5.0216963.
36. A. R. Thasneem and P. A. Subha, The switching dynamics of self-defocusing nonlinear coupled system with pt-symmetric Scarff-II barrier potential, *Eur. Phys. J. Plus* **139** (2024) 5249, https://doi.org/10.1140/epjp/s13360-024-05249-1.
37. J. Song and Z. Yan, Deep learning soliton dynamics and complex potentials recognition for 1D and 2D $\mathcal{PT}$-symmetric saturable nonlinear Schrödinger equations *Physica D* **456** (2023) 133729, https://doi.org/10.1016/j.physd.2023.133729.
38. Y.-N. Zhao and L. Feng Guo, Optical solitons of the $(2 + 1)$-dimensional nonlinear Schrödinger equation with spatio-temporal dispersion in quadratic-cubic media, *Phys. Scr.* **98** (2023) 025002, https://dx.doi.org/10.1088/1402-4896/ad0002.
39. K. Aysha Muhsina and P. Subha, Two dimensional spatial solitons in parity-time symmetric potential, *Optik* **127** (2016) 9783–9790, https://doi.org/10.1016/j.ijleo.2016.05.038.
40. X. Zhu, W. Che, Z. Wu, J. Xie and Y. He, Gap solitons supported by two-dimensional parity-time-symmetric optical lattices in saturable media with fourth-order diffraction, *J. Opt.* **22** (2020) 035503, https://iopscience.iop.org/article/10.1088/2040-8986/ab6df4.
41. Z. Shi, X. Jiang, X. Zhu and H. Li, Bright spatial solitons in defocusing kerr media with $\mathcal{PT}$-symmetric potentials, *Phys. Rev. A* **84** (2011) 053855, https://link.aps.org/doi/10.1103/PhysRevA.84.053855.
42. M. Turgut, İlkay and İBakirtaş Suppression of symmetry breaking bifurcation of solitons by fourth-order diffraction in a parity-time symmetric potential, *Chaos Solitons Fractals* **172** (2024) 112129, https://www.sciencedirect.com/science/article/pii/S0960077924008129.
43. L. Dong, M. Fan, C. Huang and B. A. Malomed, Multipole solitons in competing nonlinear media with an annular potential, *Phys. Rev. A* **108** (2023) 063501, https://link.aps.org/doi/10.1103/PhysRevA.108.063-501.

44. X. Ren and F. Deng, Dynamics of two-dimensional multi-peak solitons based on the fractional Schrödinger equation, *Fractals* **30** (2022) 2250004, https://doi.org/10.1142/S0218863522500047.
45. P. Chen and H. Wang, Two-dimensional vortex dipole solitons in nonlocal nonlinearity with pt-symmetric Scarff-II potential, *Opt. Express* **31** (2023) 30529–30540, https://opg.optica.org/oe/abstract.cfm?URI=oe-31-19-30529.
46. B. M. Zhu, X., L. Z. Mihalache and D. Xiang, Two-dimensional gap solitons in cubic-quintic nonlinear media with PT-symmetric lattices and fractional diffraction, *Eur. Phys. J. Plus* **139** (2024) 1116, https://doi.org/10.1140/epjp/s13360-024-05873-x.
47. S. S. Sastry, *Introductory Methods of Numerical Analysis* (PHI Learning, 2005), https://books.google.co.in/booksid=RhAOix1-wlYC.
48. K. Sankara Rao, *Numerical Methods for Scientists and Engineers* (PHI Learning, Delhi, 2001).
49. B. Midya, Analytical stable gaussian soliton supported by a parity-time symmetric potential with power-law nonlinearity, *Nonlinear Dyn.* **79** (2015) 273–277, https://doi.org/10.1007/s11071-014-1674-9.
50. Z. Yan, Z. Wen and C. Hang, Spatial solitons and stability in self-focusing and defocusing kerr nonlinear media with generalized parity-time-symmetric Scarff-II potentials, *Phys. Rev. E* **92** (2015) 022913, https://doi.org/10.1103/PhysRevE.92.022913.
51. B. Abdou, F. II Ndzana and L. G. Tiofack, Linear stability analysis and spatial solitons in the one-dimensional and the two-dimensional generalized nonlinear Schrödinger equation with third-order dispersion and -symmetric potentials, *Eur. Phys. J. D* **75** (2021) 34, https://doi.org/10.1140/epjd/s10053-020-00034-y.
52. J. Marcou, J. Auguste and J. Blondy, Cylindrical 2D beam propagation method for optical structures maintaining a revolution symmetry, *Opt. Fiber Technol.* **5** (1999) 187–196, https://doi.org/10.1006/ofte.1998.0283.
53. A. Abuduwali, M. Sakakihara and N. Hiroshi, A local Crank–Nicolson method for solving the heat equation, *J. Comput. Appl. Math.* **53** (1994) 75–88.
54. A. Kvaerno, Partial differential equations and finite difference methods, Lecture notes for TMA4125/4130/4135 Mathematics 4N/D, Norwegian University of Science and Technology (2020).
55. Md. Shahadat , M. N. Haquue *et al.*, Efficient finite difference methods for the numerical analysis of one-dimensional heat equation, *J. Appl. Math. Phys.* **11** (2023) 204–215, https://doi.org/10.4236/jamp.2023.1110204.
56. H. P. Langtangen and S. Linge, *Finite Difference Computing with PDEs* (Springer, 2017), https://doi.org/10.1007/978-3-319-55456-3.